Materials Chemistry and Physics 229 (2019) 482–488

Contents lists available at ScienceDirect

Materials Chemistry and Physics

journal homepage: www.elsevier.com/locate/matchemphys

Structural investigation of $La_2SrDyCu_2O_y$ complexities

M.E. Emetere[a,b,*], S.E. Sanni[a], J.T. Abodurin[a], E.E. Okoro[a], A.A. Atayero[a], A.A. Akinsiku[a]

[a] Covenant University Canaan Land, P.M.B 1023, Ota, Nigeria
[b] Department of Mechanical Engineering Science, University of Johannesburg, South Africa

HIGHLIGHTS

- The potential of structural modification was examined.
- Ii. A predefined polycrystalline LSDCO structure was fabricated.
- Iii. The primary and secondary phase interaction was examined.
- Iv. The transport analysis of heavy ions within LSDCO was investigated.
- The surface scan and XRD was used to explain the sample bounaries.

ARTICLE INFO

Keywords:
Cuprates
High temperature superconductor
Lattice
LSDCO
Structural modulation

ABSTRACT

The structural complexities in lanthanum cuprates family were revisited with the aim of understanding factors that structurally triggers long-range repulsive Coulomb interactions. In this study, polycrystalline samples of $La_2SrDyCu_2O_y$ (LSDCO) were prepared via solid-state synthesis using high purity chemicals. The X-ray diffraction experiment revealed an unusual structural anomaly in the [2 0 5] and [2 1 3] planes of the crystal lattice. The lattice system was further probed using the Niggli-reduced cell at gamma = 6.0678. It was observed that grain boundaries leading to electron trapping originates from the CuO_2 plane while the mesoscopic phase separation is controlled by the cell type and axial value in the x- and y-axes of the crystal lattice. Although the research partly supports popular findings that the main positive lobes of LSDCO are centered on the z-axis, it observed that the negative lobe is located in a ring-like structure along the X−Y plane. This result is particularly interesting because it shows the likely origin of broken symmetry in LSDCO sample. The ion bombardment analysis shows that the LSDCO electron-phonon ratio was 8:5. The microstructural analysis of the LSDCO sample was observed to have magnetic field strength of 1.5 kA/m. LSDCO sample possess enormous structural mystery that may interest further studies beyond superconductivity.

1. Introduction

The effect of structural complexities on the long-range repulsive Coulomb interaction and how it influences the charge ordering and wave vector of the ordering transitions is becoming clearer by the day [1]. Chen et al. [2] showed the relationship between the long-range Coulomb force of an atomic structure and its effect on volume fraction, coordination number as well as the radial distribution function of its packing structure. One of the highlights of the study is that long-range Coulomb interaction enables loose/weaker packing structure via its influence on the particle inertia. More so, scientists have shown that long-range Coulomb interaction gives rise to mesoscopic phase separation [3–5]. Yukalov and Yukalova [6] worked on anisotropic superconductors. Their findings show that the mesoscopic phase of an anisotropic superconductor enhances superconductivity in the heterophase. Till date, the physics that links the mesoscopic phase separation to other microscopic events in cuprates is still unclear.

Lanthanum cuprates compound was chosen in this study because of its spin properties, charge-order splitting capabilities [7,8] and bilayer splitting in the band structure [9]. Seibold et al. [10] observed that the orthorhombic lattice distortion in lanthanum has significant effect on the magnetic scattering along the orthorhombic b-axis. The explanation for this event may be linked to the displaced atoms within the lattices that engender local correlations of several lattice constants. Sarrao et al. [11] supported this assertion via La NMR study that two magnetically distinct sites (i.e. charged stripe and intervening hole-free domains) emerge from charge ordering. More so, doping the lanthanum cuprates with rare earth ions induces the low temperature tetragonal (LTT)

* Corresponding author. Covenant University Canaan Land, P.M.B 1023, Ota, Nigeria.
E-mail address: emetere@yahoo.com (M.E. Emetere).

https://doi.org/10.1016/j.matchemphys.2019.03.052
Received 31 January 2019; Received in revised form 14 March 2019; Accepted 15 March 2019
Available online 16 March 2019

phase that has been proven to initiate pinning of the stripe fluctuations [12]. For example, a small concentration of Gd supports pair breaking and creates significant influence on the critical temperature and nuclear spin-lattice relaxation in lanthanum compounds [13]. Also, it has been discovered that when lanthanum cuprates are doped with rare earth metals, it produce static charge stripes [14].

From the report of Hammel et al. [14] on the role of charge localization, it implies that there exist local inhomogeneities in crystal structures that do not originate from distortions of the dopants. It was reported that local inhomogeneities in the crystal lattice of a superconductor might arise from the intrinsic response of the CuO_2 planes to the presence of doped holes. Ultimately, this event leads to inhomogeneous distribution of charges in the CuO_2-planes because of the presence of complex layered lattices or uneven heterogeneous lattices and ions or atoms alongside unpaired electrons or electrons not included in closed shells [15]. However, the misunderstanding of the above, lies within the lattice discontinuities found at the borders between cells with different ionic compositions. Hence, in this research, the focus is to parametrically estimate the structural instability in a highly inhomogeneous lanthanum cuprate ($La_2SrDyCu_2O_y$). This view opposes some earlier assertions that the key factors in creating and destroying the superconducting state includes temperature, magnetic field, doping and atomic substitution [16,17]. All these factors are not consistent because of emerging lattice complexities. For example, a rich spatial complexity of the two classes of electronic states in underdoped cuprates was first revealed using the spectroscopic imaging scanning tunneling microscopy [34]. The above discovery shows that broken symmetry is a dynamic concept, especially when some scientists believe that the broken symmetry states interact with the superconducting components of the CuO_2 electronic structure [35]. The second example of structural complexity in cuprates sample is evident when reducing the thickness of thin film $SrCuO_2$ to create a chain-type structure from its original planar-type structure [31]. Hence, structural complexities in cuprates material have huge effect on the electronics and transport properties of the compounds. This fact was partly proven when the microstructural modifications of lanthanum compounds were examined [32]. Furthermore, the new concept behind the fabrication of new copper oxide superconductor Ba2CuO_4 with 214 type structure is linked to the structural complexities in the cuprates compounds [33]. Hence, there is the need to carry-out a parametric study on the structural complexities of LSDCO to understand the possible occurring events.

2. Material and methods

The polycrystalline samples of $La_2SrDyCu_2O_y$ were prepared by solid state synthesis using high purity chemicals of $La(NO_3)_3.6H_2O$, $Sr(NO_3)_2$, $Dy(NO_3)_3.6H_2O$, $Cu(NO_3)_2.3H_2O$, Citric acid and Ethylene Glycol (> 99.9% purity and made by Sigma Aldrich) [32]. The chemicals were weighed using an electronic balance as stipulated in the stoichiometric amounts i.e. $La_2SrDyCu_2O_y$. The stoichiometric value 'y' stands for amount oxygen that is derivable from the aforementioned chemicals. Each of the samples was mixed/diluted with 10 ml of distilled water inside a 100 ml beaker. The mixture was properly mixed by heating the compounds at 100 °C and stirred continuously on a digital mixer set at 800 rpm for 75 min. Polyesterification of the homogenous blue solution was then carried out at 350 °C for 2 h. The resulting was grinded to smooth powder. The product was calcined for 5.5 h in air at 800 °C and a black powder was obtained. The vigorous reaction that ensued from the process caused the splashing of the components out of the covered-crucible. Consequently, the partly fine powder was ground the second time using the agate mortar. The powder obtained was formed into cylindrical pellets under a pressure of 13 kN at room temperature for 7 min. The pellet was sintered at 850 °C for 1 h and cooled in air at room temperature. The pellet was sintered the second time at 850 °C for 16 h in order to further coalesce the solid fines. The sample was then allowed to cool in air at room temperature. he sample was synthesize and characterized at University of Johannesburg and University of South Africa.

Phase analysis of the sample was done at room temperature using X-ray diffraction (XRD) on a Siemens D8-Advance powder diffractometer at Cu-Ka radiation wavelength of $\lambda = 1.5418$°A with an angle step of 0.021. Microstructural examinations of the samples were done using a scanning electron microscopy (SEM). An in-depth analysis of the bond and structural complications of the SEM images were analyzed. The ion bombardment analysis was carried-out using 99,999 ions bombardments on the sample.

3. Results and discussion

The XRD results showing the phase in LSDCO are presented in Fig. 1. It can be inferred that the sample has an orthorhombic structure with a space group of I 4/m m m. This observation makes it possible for the sample to have orthorhombic lattice distortion (OLD). OLD has been linked to elastic diagonal magnetic scattering [10]. The refinement of the XRD data shows that it has specimen displacement correction (Bragg-Brentano geometry) of T = (-s/R) = 0.00074972 at a wavelength of 1.540598 Å. The peaks were seen to correspond to existing crystal phase database [18–21] using the Match software. The excess oxide removal was done as presented in Fig. 2. The phase identification of the elemental composition of LSDCO was documented from online crystal database. The analysis is presented in Fig. 3. The most prominent hkl planes with higher frequency are shown on the x-axis of Fig. 3. The [2 0 5] plane in the LSDCO was the only prominent plane among the individual elements of LSDCO that corresponds with XRD refinement shown in Fig. 1. The [2 0 5] and [2 1 3] planes correspond to Sr—La—Cu_3 and Sr—La lattice framework. This event may be a positive indication that lattice strain may likely occur in the LSDCO sample. T.

The lattice system was transformed into the Niggli-reduced cell at gamma = 6.0678 (Table 1). The calculation was based on an ionic sphere radius of 2.65 Å; reciprocal-space range of 1.25 Å; number of symmetry operations equal to 16; number of atoms in the asymmetric unit is equal to 13; and inversion center at the origin as 1. The Niggli-reduction technique helps to understand the complexities in Bravais lattice identification and complex space that have not previously been fully analyzed [22,23]. In Table 1, six oxygen atoms, two copper atoms, two lanthanum atoms and one strontium and dysprosium were transformed. It was observed that only strontium had a different cell type with a high axial value in the x- and y-axes. The O1 interaction with O6 oxygen atoms was abnormally high compared to other oxygen atom present. Hence, the complexity of the interactions of similar atoms, such as, those of oxygen, is somewhat unique. It was observed that 75% of the participating atoms had same x- and y-coordinates (e.g. O2/O1, O3/O5, O4/O3, Dy/Dy1, O5/O2, Cu2/Cu2, La1/La2, O6/O1, and Sr/Sr1) while the variation of the atoms lies along the z-axis. Therefore, in part it supports Ref [26], that is, the main positive lobes of LSDCO are centered on the z-axis while, the negative lobe is located in a ring-like structure along the X—Y plane. In same vein, there were few atoms that had dynamic values in the x-, y- and z-axes as seen in Table 1.

It is unclear if the ring-like structure may still exist in a changing axial position. Hence, the potentials of sites in the asymmetric were considered as presented in Table 2. Here, the electrostatic energy per asymmetric unit is given as −2.298601, $e^2/Å = -33.09905$ and eV = −3.193572 MJ/mol at unit cell volume of 297.076469 $Å^3$. It was observed that Sr, La and O1 had different work function W. Thus, this result confirmed the occurrence of a unique event -occurring in the Sr and La atoms along the [2 0 5] and [2 1 3] coordinates. All calculations

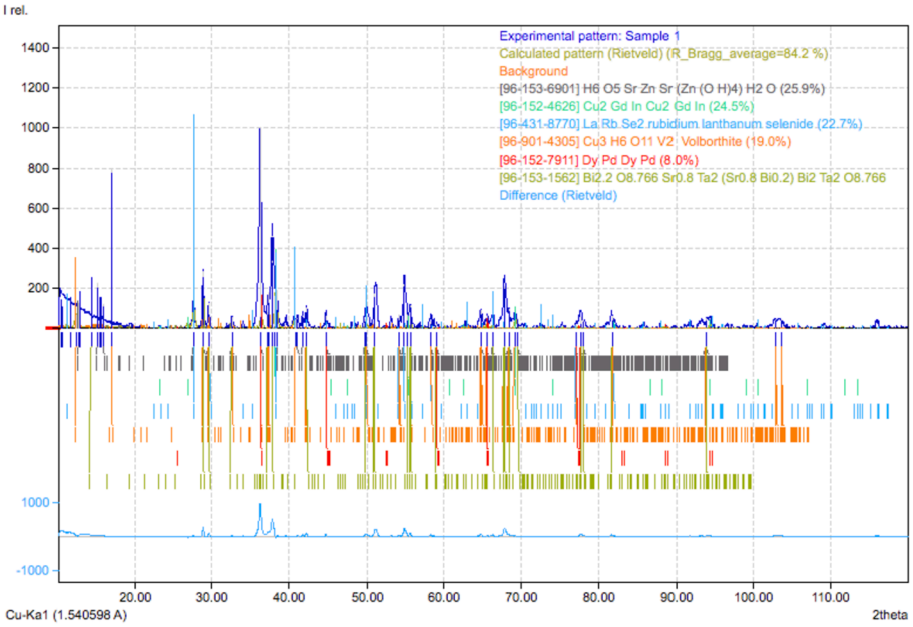

Fig. 1. XRD patterns of $La_{2x}Sr_xDy_xCu_{2x}O_y$.

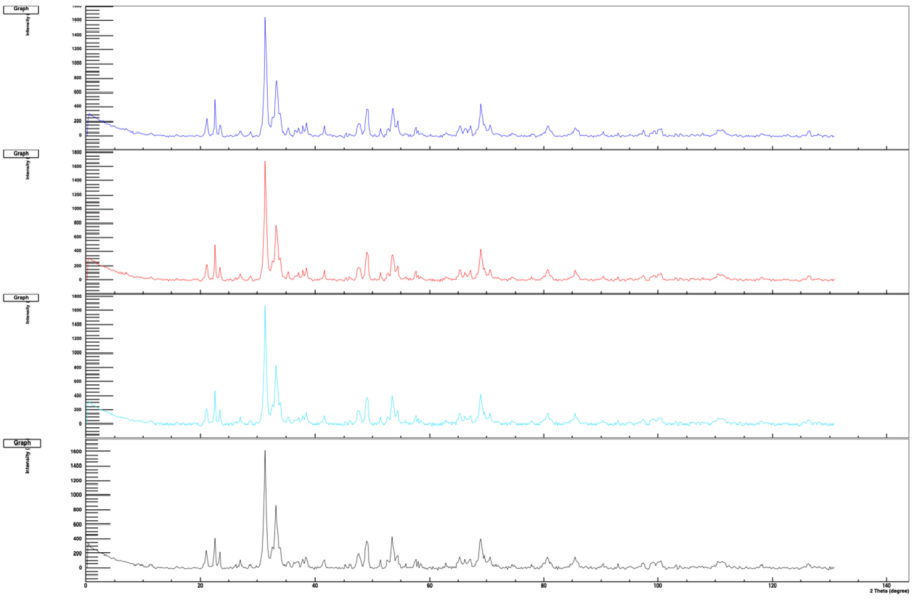

Fig. 2. Excess oxide removal from LSDCO.

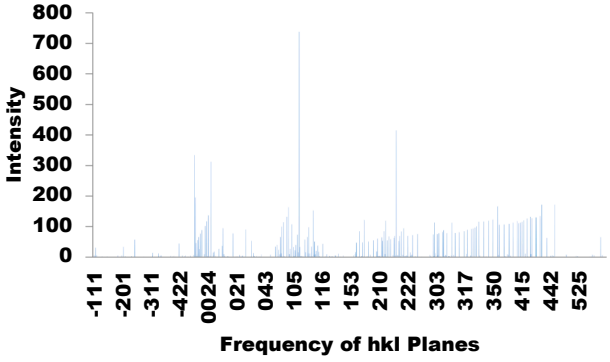

Fig. 3. Intensity of individual LSDCO elements.

presented in Table 2 occurred solely along the z-axis. The Rietveld refinement of the XRD data shows that the Bragg R-factor ranges from 73.71 to 88.78 while the RF factor ranges from 47.2 to 62.45. Hence, aside the mystery in the CuO plane, there exists the mystery that La and Sr may be either complimentary or opposing at some point in the lattice of the lanthanum cuprates.

The higher the number of oxygen atoms, the better the coordination number (Table 1). The highest and least phi values of strontium and lanthanum molecules exhibit similar x, y, z coordinates but different work functions and charges as presented in Table 2.

The five patterns of structural interactions noticed at the a-, b-, and c-axes were presented in Table 3. The interatomic bond angles along the a-, b-, and c-axes showed varying shapes that suggest instability in the cuprates system. Some scientists have argued that the instability of the cuprates system enhances superconductivity in a way [24,25]. However, it is still unclear if these instabilities lead to charge-lattice

Table 1
Transformation to a Niggli-reduced cell (gamma = 6.0678).

Atom	Cell	x	y	z	Atom
O1	2(i)	10.3122	100.801	100.801	O6
O2	2(i)	0.01500	0.01500	0.03000	O1
Cu1	2(i)	0.08400	0.58400	0.16800	Cu1
O3	2(i)	0.09130	0.09130	0.18260	O5
O4	2(i)	0.09500	0.09500	0.19000	O3
Dy	2(i)	0.19500	0.19500	0.39000	Dy1
O5	2(i)	0.20000	0.20000	0.40000	O2
Cu2	2(i)	0.20500	0.20500	0.41000	Cu2
La1	2(i)	0.20870	0.20870	0.41740	La2
O6	2(i)	0.32170	0.32170	0.64340	O1
La2	2(i)	0.58400	0.08400	0.16800	La1
Sr	1(e)	0.60000	0.60000	0.20000	Sr1

Table 2
Potentials of sites in the asymmetric unit.

Atom	Charge	W	x	y	z	Phi
La1	3.000	0.0625	0.000	0.000	0.400000	−2.880383E+00
Sr1	2.000	0.0312	0.000	0.000	0.500000	−3.897751E+00
La2	3.000	0.0938	0.000	0.000	0.321700	−6.073118E-03
Sr2	2.000	0.0312	0.000	0.000	0.321700	9.844929E-01
Cu1	2.000	0.1250	0.000	0.000	0.091300	−3.817906E+00
O1	−2.000	0.2500	0.000	0.000	0.084000	2.539933E-01
O2	−2.000	0.1250	0.000	0.000	0.205000	3.915997E+00
Dy1	3.000	0.1250	0.000	0.000	0.200000	−1.166597E+00
Cu2	2.000	0.1250	0.000	0.000	0.208700	4.758721E-02
O3	−2.000	0.1250	0.000	0.000	0.195000	3.653257E+00
O4	−2.000	0.1250	0.000	0.000	0.195000	3.653257E+00
O5	−2.000	0.1250	0.000	0.000	0.095000	2.862773E-01
O6	−2.000	0.1250	0.000	0.000	0.015000	−2.042456E+00

ordering, electron-lattice ordering, electron-phonon interaction etc. Dy, La, and Cu had high magnitude along the interatomic bonding angles while O and Sr had low magnitude along the interatomic bonding angles. The structural changes in the LSDCO sample along the a-, b- and c-axes are presented in Fig. 4.

Dy element was observed to play specific role in the structural formation in the a-b-c axes (i.e. along the b-c axes, Dy, La, Sr are prominent, along a-c axes, Dy, La, Sr are prominent, along a-b-c axes, Dy, Cu and Sr are prominent, along a-b axes, Dy and Sr and Cu are prominent along b-c axes) shows how individual elements could determine the structural complexities in a material. This means that the properties of dysprosium (creation of magnetic susceptibility in the pseudogap phase) may have unique role in the lattice displacement of the LSDCO sample.

The SEM image is presented in Fig. 5. The analysis of the surface structure using the Gywddion software is presented in Fig. 6. Fig. 6

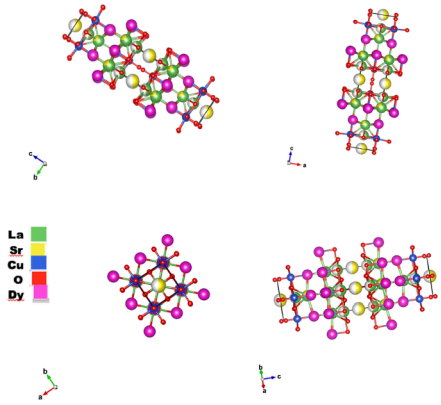

Fig. 4. Structural variation of the LSDCO along a-, b- and c-axes.

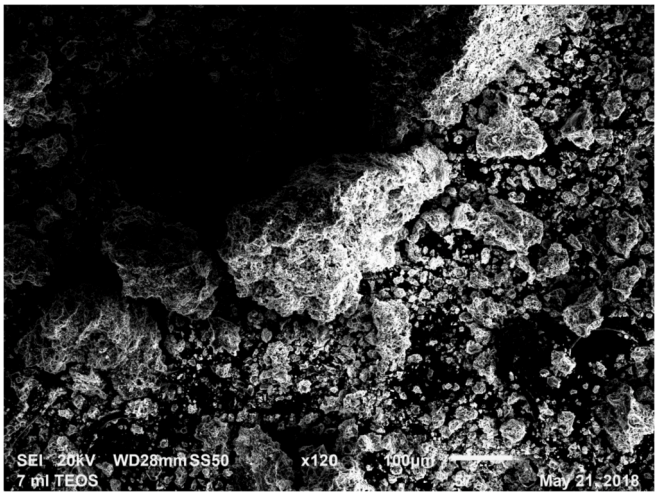

Fig. 5. Scanning electron microscope image of LSDCO.

show typically the 3D image of the lattice system of LSDCO. The detailed Gwyddion analysis of SEM images is presented in Ref. [32]. The red dots in the diagram presents the energy levels in the compound. Electrons “jump” from one energy level to another in a few nanoseconds or less. The blue line represents the grain boundaries that electrons are expected to tunnel through as explained by Nguyen et al. [27]. The electron mobility in the LSDCO was examined in three scenarios i.e. in its pure form (Fig. 6a), in its optimized form (Fig. 6b) and when the background is removed (Fig. 6c). The pure LSDCO sample has grain boundary formation that has the ability to trap electron mobility at specified sections of the lattice (Fig. 6a). It is believed that the presence

Table 3
Interatomic bond angles along the a-, b-, and c-axes of LSDCO.

La			Sr			Cu		
a	b	c	a	b	c	a	b	c
19.966	3.197	−21.745	17.730	1.563	1.140	14.014	3.738	−3.254
27.330	0.003	−21.745	9.796	14.311	1.140	4.785	0.004	−3.254
11.018	19.955	−21.745	6.100	0.121	1.140	5.057	13.035	−3.254
3.087	141.382	−21.745	2.620	135.771	1.140	1.458	72.555	−3.254
17.335	0.342	−21.745	0.600	0.121	1.140	6.933	0.266	−3.254
Dt			O					
a	b	c	a	b	c			
26.672	2.283	−83.280	2.960	14.182	0.027			
88.688	0.001	−83.280	2.509	5.937	0.027			
14.065	12.920	−83.280	0.638	0.113	0.027			
2.768	121.937	−83.280	0.723	34.958	0.027			
17.068	0.226	−83.280	1.143	0.390	0.027			

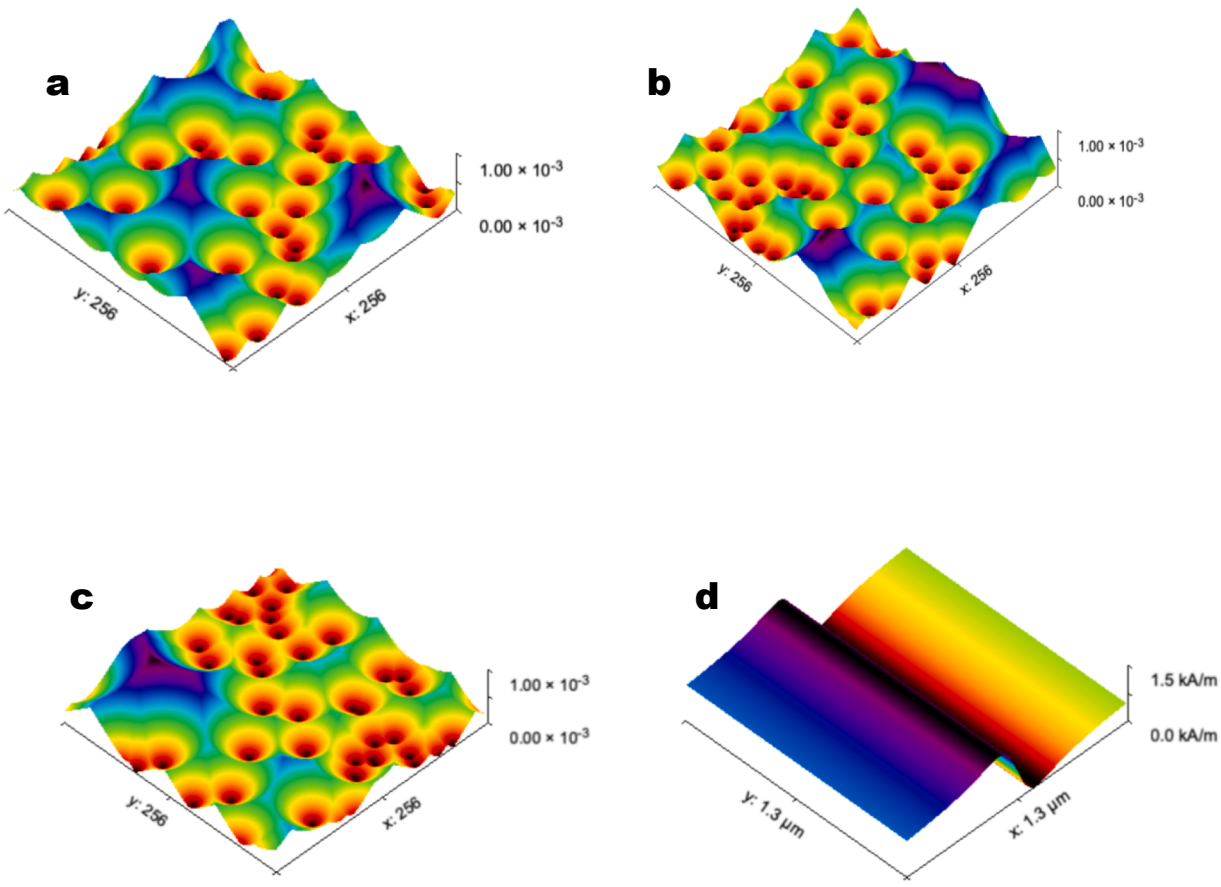

Fig. 6. The analyzed SEM image of the LSDCO sample showing different energy levels and grain boundaries.

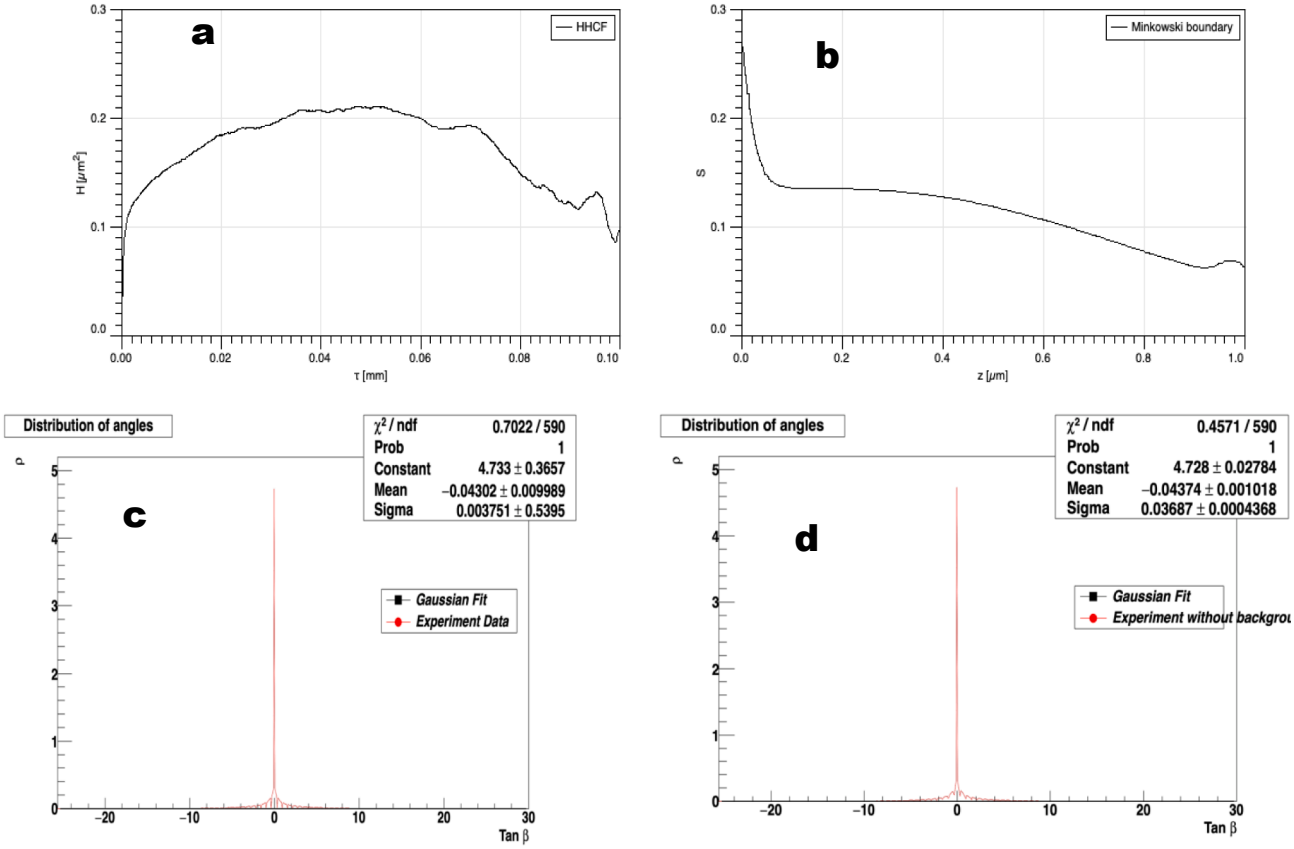

Fig. 7. Grain size characterization of the LSDCO sample.

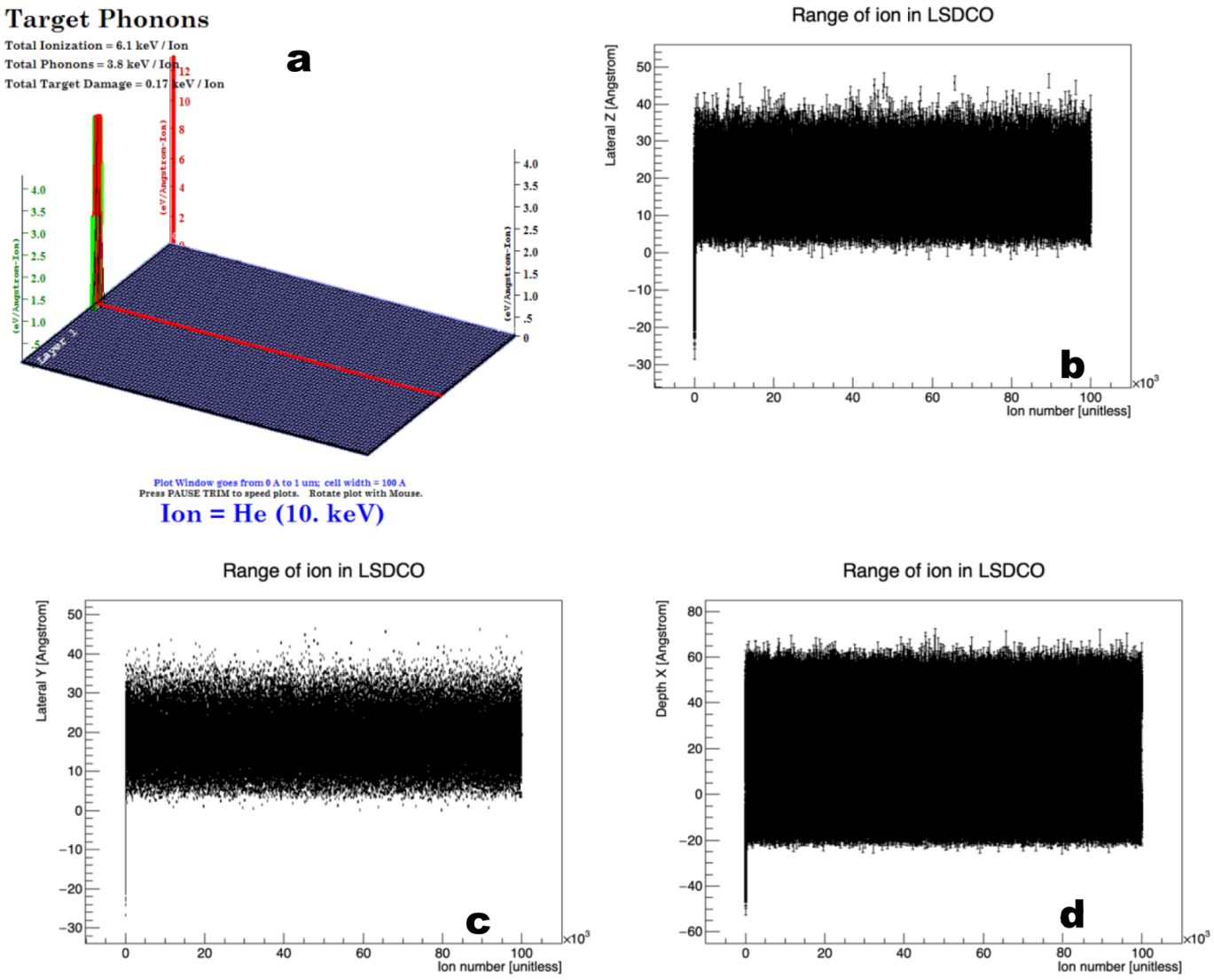

Fig. 8. Analyses of the ions in the LSDCO sample.

of adsorbed oxygen species in the grain boundaries have significant role on its electron mobility [28,29]. The surface of the scan was theoretically optimized applying the magnetic field shift in the z-axis; hence, the reduction of the electron mobility traps as presented in Fig. 6b. Based on the above, it is logical to ask i.e. where does the adsorbed oxygen originate? In this case the background was subtracted from the LSDCO sample using the Gywddion software as presented in Fig. 6c. The background of the SEM image is believed to be the CuO_2 plane. It was observed that grain boundaries leading to electron trapping originated from the CuO_2 plane. Since superconductivity is triggered in the CuO_2 plane, the magnetic field strength at the LSDCO surface was estimated in Fig. 6d to be 1.5 kA/m.

The analysis of the LSDCO surface is critical. The height-height correlation function (HHCF) obtained for a simulated Gaussian surface is presented in Fig. 7a. Thus, it can be inferred that there is the formation of asymmetric grains within the sample. Scientists have shown that asymmetric dust grains have the tendency to align within a magnetic field [30]. Perhaps that is why its maximum magnetic field strength was as high (1.5 kA/m). More so, such material exhibits the Ehrlich-Schwoebel-like energy barrier that naturally breaks the growth symmetry (Fig. 7a). The Minkowski boundaries show that the LSDCO has wide range of values (i.e. from 0.8 to 2.7) that subsequently affirm the complexity of the material (Fig. 7b). However, the distribution of scanning angle as presented in Fig. 7c shows a Gaussian shape with rough curves. This suggests the presence of adsorbed oxygen in the sample. The statistical information is shown in the inset of the diagram. Also, the distribution of scanning angle for a LSDCO sample without background was plotted as presented in Fig. 7d. The statistical analyses in the inset of the plot show the significance of the Cu—O planes in the LSDCO sample.

The electron-phonon interaction was estimated via the ion bombardment analysis that was carried-out using the SRIM software. The sample was ionized with the Helium source of 10 keV. It was observed that the LSDCO sample had electron-phonon ratio of 8:5 (Fig. 8a). The bombardment of 99999 ions was incident unto the sample. The analyses of ions along the lateral z (Fig. 8b), lateral y (Fig. 8c) and depth x (Fig. 8d) clearly show the effect of grain boundaries. For example, electron mobility will be easier along depth x. More so, it also shows that the grain boundaries in the sample are somewhat two-dimensional, as it possesses almost the same lattice length in the lateral z and y directions.

4. Conclusion

The Structural displacements in the formed LSDCO system were found to be dynamic due to the structural complexities noticed in the [2 0 5] and [2 1 3] planes of the crystal lattice. The lattice system was transformed into Niggli-reduced cell at gamma = 6.0678. The

interactions between similar atoms of oxygen have its unique role to enhance or destroy superconductivity. Positive lobes of LSDCO were found to be centered on the z-axis while negative lobes were confined in a ring-like structure along the X−Y plane. This result is particularly interesting because it shows the likely origin of broken symmetry in LSDCO sample. This assertion was corroborated by the wide range values of the Minkowski boundaries. Hence, it is believed that the position of the positive and negative lobes may interchange at some stage. It was also observed that the Sr and La atoms have unique contribution to the sample at the [2 0 5] and [2 1 3] planes. Patterns of structural interactions was observed at the a, b, c axes. It revealed that the interatomic bond angles along the axes showed varying shapes that indicate instabilities in the cuprates system. Dy, La, and Cu showed high instabilities in their interatomic bonding angles while O and Sr had low instabilities along the interatomic bonding angles. Along the a-b axes, Dy and Sr and Cu were found most prominent i.e. the properties of dysprosium (creation of magnetic susceptibility in the pseudogap phase) could have had influence on the lattice displacement inherent in the LSDCO sample i.e. confirming the presence of Dy in all paired axes. The microstructural analysis of the LSDCO sample gave an estimated magnetic field strength of 1.5 kA/m. Based on the height-height correlation function (HHCF) that was obtained for the simulated Gaussian surface of the cuprate system, it can be inferred that there is the formation of asymmetric grains within the sample. Hence, the likely reason for electron-phonon ratio of 8:5 in the LSDCO sample.

Acknowledgement

The authors wish to acknowledge the above-listed institutions.

References

[1] C. Ortix, J. Lorenzana, C. Di Castro, Coulomb-Frustrated phase separation phase diagram in systems with short-range negative compressibility, Phys. Rev. Lett. 100 (2008) 246402.
[2] S. Chen, S. Li, W. Liu, H.A. Makse, Effect of long-range repulsive Coulomb interactions on packing structure of adhesive particles, Soft Matter 12 (6) (2016) 1836–1846.
[3] J. Lorenzana, C. Castellani, C. Di Castro, Phase separation frustrated by the long-range Coulomb interaction I, Theory Phys. Rev. B 64 (2001) 235127.
[4] S.A. Kivelson, I.P. Bindloss, E. Fradkin, V. Oganesyan, J.M. Tranquada, A. Kapitulnik, C. Howald, How to detect fluctuating stripes in the high-temperature superconductors, Rev. Mod. Phys. 75 (2003) 1201.
[5] V.I. Yukalov, Phase transitions and heterophase fluctuations, Phys. Rep. 208 (1991) 395–489.
[6] V.I. Yukalov, E.P. Yukalova, Mesoscopic phase separation in anisotropic superconductors, Phys. Rev. B 70 (2004) 224516.
[7] J.M. Tranquada, J.D. Axe, N. Ichikawa, Y. Nakamura, S. Uchida, B. Nachumi, Neutron-scattering study of stripe-phase order of holes and spins in $La_{1.48}Nd_{0.4}Sr_{0.12}CuO_4$, Phys. Rev. B 54 (1996) 7489.
[8] J.M. Tranquada, J.D. Axe, N. Ichikawa, A.R. Moodenbaugh, Y. Nakamura, S. Uchida, Coexistence of, and competition between, superconductivity and charge-stripe order in $La_{1.6-x}Nd_{0.4}Sr_xCuO_4$, Phys. Rev. Lett. 78 (1997) 338.
[9] D.L. Feng, N.P. Armitage, D.H. Lu, A. Damascelli, J.P. Hu, P. Bogdanov, A. Lanzara, F. Ronning, J.-i. Shimoyama, K. Kishio, Bilayer splitting in the electronic structure of heavily overdoped Bi2Sr2CaCu2O8 + δ, Phys. Rev. Lett. 86 (2001) 5550.
[10] G. Seibold, M. Grilli, J. Lorenzana, Stripes in Cuprate Superconductors: Excitations and Dynamic Dichotomy, (2012) arXiv:1202.1615v1 [cond-mat.str-el].
[11] J.L. Sarrao, D.P. Young, Z. Fisk, E.G. Moshopoulou, J.D. Thompson, B.C. Chakoumakos, S.E. Nagler, Structural, magnetic, and transport properties of $La_2Cu_{1-x}Li_xO_4$, *Phys. Rev.* B 54 (1996) 12014.
[12] J.M. Tranquada, B.J. Sternlieb, J.D. Axe, Y. Nakamura, S. Uchida, Evidence for stripe correlations of spins and holes in copper oxide superconductors, Nature 375 (1995) 561.
[13] G.B. Teitel'Baum, V.E. Kataev, E.L. Vavilova, P.L. Kuhns, A.P. Reyes, W.G. Moulton, Magnetic phase separation in $La_{1-x}SrxCoO3$ by ^{59}Co nuclear magnetic resonance, Phys. Rev. Lett. 91 (2003) 127202.
[14] P. Chris Hammel, et al., Role of charge localization in the basic high temperature superconductivity mechanism, http://lib-www.lanl.gov/la-pubs/00818568.pdf.
[15] V. Maxia Brovetto1, M. Salis, On the Theory of High Temperature Superconductivity, (2003) arXiv:cond-mat/0312015v2 [cond-mat.supr-con].
[16] M.E. Emetere, Profiling laser induced temperature fields for superconducting materials using mathematical experimentation, J. Thermophys. Heat Transf. 28 (4) (2014) 700–707, https://doi.org/10.2514/1. T4407.
[17] M.E. Emetere, Characteristic significance of magnetic relaxations on copper oxide thin film using the bloch NMR, Surf. Rev. Lett. 21 (5) (2014) 1450075, https://doi.org/10.1142/S0218625X14500759.
[18] B.E. Zaitsev, B.N. Ivanov-Emin, L.P. Petrishcheva, A.M. Ilinets, N.A. Baturin, L.L. Regel, Ik spectrum of sodium and alkali earth metals hydroxozincates and crystal structure of $SrZn(OH)_4\ H_2O$, *KoordinatsionnayaKhimiya* (= Coordination Chemistry (USSR)) 16 (1990) 1255–1259.
[19] B. Deng, E. Donald, D.E. Ellis, J.A. Ibers, New layered rubidium rare earth selenides: syntheses, structures, physical properties, and electronic structures for $RbLnSe_2$, Inorg. Chem. 41 (22) (2002) 5716–5720, https://doi.org/10.1021/ic020324j.
[20] H. Yoshida, J. Yamaura, M. Isobe, G.J. Nilsen, Z. Hiroi, Orbital switching in a frustrated magnet, Nat. Commun. 3 (2012) 860865.
[21] A. Palenzona, S. Cirafici, Thermodynamic and crystallographic properties of Re, Pd intermetalliccompounds, Thermochim. Acta 12 (1975) 267275.
[22] M. Hosoya, A finite group that derives all the 14 Bravais lattices as its subgroups, Acta Crystallogr. 56 (3) (2000) 259–263.
[23] R. Oishi-Tomiyasu, Rapid Bravais-lattice determination algorithm for lattice parameters containing large observation errors, Acta Crystallogr. 68 (5) (2012) 525–535.
[24] H. Oyanagi, C.J. Zhang, Lattice instability in high temperature superconducting cuprates and FeAs systems: polarons probed by EXAFS, Adv. Condens. Matter Phys. (2010) 10 2010: 484578 https://doi.org/10.1155/2010/484578.
[25] E.H. da Silva Neto, P. Aynajian, A. Frano, R. Comin, E. Schierle, E. Weschke, A. Gyenis, J. Wen, J. Schneeloch, Z. Xu, S. Ono, G. Gu, M.L. Tacon, A. Yazdani, Ubiquitous interplay between charge ordering and high-temperature superconductivity in cuprates, Science 343 (2014) 393–396.
[26] M.E. Emetere, Effects of tunable bloch inspired spin orbit interaction in the electronic state of Sr_2RuO_4, J. Supercond. Nov. Magnetism 27 (10) (2014) 231–239, https://doi.org/10.1007/s10948-014-2848-x.
[27] V.H. Nguyen, U. Gottlieb, A. Valla, D. Munoz, D. Bellet, D. Munoz-Rojas, Electron tunneling through grain boundaries in transparent conductive oxides and implications for electrical conductivity: the case of ZnO: Al thin films, Materials Horizon 4 (2018).
[28] K.E. Lee, M. Wang, E.J. Kim, S.H. Hahn, Structural, electrical and optical properties of solegel AZO thin films, Curr. Appl. Phys. 9 (2009) 683–687.
[29] V.V. Titov, A.A. Lisachenko, I.K. Akopyan, M.E. Labzowskaya, B.V. Novikov, J. Lumin, On the nature of the effect of adsorbed oxygen on the excitonic photoluminescence of ZnO, J. Lumin. 195 (2018) 153–158.
[30] B.-G. Andersson, Magnetic fields in diffuse media, Astrophys. Space Sci. Libr. 407 (2015) 627.
[31] J.W. Harter, et al., Doping evolution and polar surface reconstruction of the infinite-layer cuprate Sr1 − xLaxCuO2, Phys. Rev. B 92 (2015) 035149.
[32] M.E. Emetere, T.W.P. Seadira, M. Madhuku, M.E. Segale, Investigating the structural modifications in LaAlYbCuO, Results in Physics 12 (2019) 1628–1644.
[33] W.M. Li, L.P. Cao, J.F. Zhao, R.Z. Yu, J. Zhang, Y. Liu, Q.Q. Liu, G.Q. Zhao, X.C. Wang, Z. Hu, Q.Z. Huang, H. Wu, H.J. Lin, C.T. Chen, J.S. Kim, G. Steward, Z. Li, Y.W. Long, Z.Z. Gong, Z. Guguchia, Y.J. Uemura, S. Uchida, C.Q. Jin, A New Superconductor of Cuprates with Unique Features, (2019) arXiv:1808.09425 [cond-mat.supr-con].
[34] Jhinhwan Lee, et al., Spectroscopic Signature of Phase Incoherent Superconductivity in Underdoped Bi2Sr2CaCu2O8 + δ Science vol. 325, (2009), pp. 1099–1103.
[35] A.R. Schmidt, K. Fujita, E.-A. Kim, M.J. Lawler, H. Eisaki, S. Uchida, D.-H. Lee, J.C. Davis, Electronic structure of the cuprate superconducting and pseudogap phases from spectroscopic imaging STM, New J. Phys. 13 (2011) 065014.